Unstable modes and bistability in delay-coupled swarms

Jason Hindes, Victoria Edwards, Sayomi Kamimoto, Ioana Triandaf, and Ira B. Schwartz

Phys. Rev. E **101**, 042202 — Published 6 April 2020

DOI: 10.1103/PhysRevE.101.042202

Unstable modes and bistability in delay-coupled swarms

Jason Hindes[1], Victoria Edwards[2], Sayomi Kamimoto[3], Ioana Triandaf[1], and Ira B. Schwartz[1]
[1] *U.S. Naval Research Laboratory, Code 6792, Plasma Physics Division, Washington, DC 20375, USA*
[2] *U.S. Naval Research Laboratory, Code 5514, Navy Center for Applied Research in Artificial Intelligence, Washington, DC 20375, USA and*
[3] *Department of Mathematics, George Mason University, Fairfax Virginia, 22030, USA*

It is known that introducing time delays into the communication network of mobile-agent swarms produces coherent rotational patterns, from both theory and experiments. Often such spatio-temporal rotations can be bistable with other swarming patterns, such as milling and flocking. Yet, most known bifurcation results related to delay-coupled swarms rely on inaccurate mean-field techniques. As a consequence, the utility of applying macroscopic theory as a guide for predicting and controlling swarms of mobile robots has been limited. To overcome this limitation, we perform an exact stability analysis of two primary swarming patterns in a general model with time-delayed interactions. By correctly identifying the relevant spatio-temporal modes, we are able to accurately predict unstable oscillations beyond the mean-field dynamics and bistability in large swarms– laying the groundwork for comparisons to robotics experiments.

I. INTRODUCTION

In nature, swarms consist of individual agents with limited dynamics and simple rules, which interact, sense, collaborate and actuate to produce emergent spatio-temporal patterns. Examples include schools of fish[1–3], flocks of starlings[4, 5] and jackdaws[6], colonies of bees[7], ants[8], locusts[9], and bacteria[10], as well as crowds of people[11]. Given the many examples across a wide range of space and time scales, significant progress has been made in understanding swarming by studying simple dynamical models with general properties[12–14].

Deriving inspiration from nature, embodied artificial swarm systems have been created to mimic emergent pattern formation– with the ultimate goal of designing robotic swarms that can perform complex tasks *autonomously*[15–18]. Recently robotic swarms have been used experimentally for applications such as mapping[19], leader-following[20, 21], and density control[22]. To achieve swarming behavior, often, robots are controlled based on models, where swarm properties can be predicted exactly[23–27]. Such approaches rely on strict assumptions to guarantee behavior. Any uncharacterized dynamics can cause patterns to be lost or changed. This is particularly the case for robotic swarms that move in uncertain environments and must satisfy realistic communication constraints.

In particular in both robotic and biological swarms, there is often a delay between the time information is perceived and the reaction time of agents. Such delays have been measured in swarms of bats[28], birds[29], fish[30], and crowds of people[31]. Delays naturally occur in robotic swarms communicating over wireless networks, due to low bandwidth[32] and multi-hop communication[33]. In general, time-delays in swarms result in multi-stability of rotational patterns in space, and the possibility of switching between patterns[34–42]. Though observed in simulations and experiments, swarm bistability due to time-delay has lacked an accurate quantitative description, which we provide in this work.

Consider a system of mobile agents, or swarmers, moving under the influence of three forces: self-propulsion, friction, and mutual attraction. In the absence of attraction, each swarmer tends to a fixed speed, which balances propulsion and friction but has no preferred direction. The agents are assumed to communicate through a network with time delays. Namely, each agent is attracted to where its neighbors were at some moment in the past. A simple model which captures the basic physics is

$$m\ddot{\mathbf{r}}_l = \left[\alpha - \beta|\dot{\mathbf{r}}_l|^2\right]\dot{\mathbf{r}}_l + \frac{a}{N-1}\sum_{j\neq l}[\mathbf{r}_j(t-\tau) - \mathbf{r}_l] + \boldsymbol{\xi}_l(t). \tag{1}$$

where m is the mass of each agent, α is a self-propulsion constant, β is a friction constant, a is a coupling constant, τ is a characteristic time delay, N is the number of agents, $\mathbf{r}_l$ is the position-vector for the lth agent in two spatial dimensions, and $\boldsymbol{\xi}_l(t)$ is a small noise source[34, 43–46]. Equation (1) has been implemented in experiments with several robotics platforms including autonomous cars, boats, and quad-rotors[35, 36]. Note: in this work we consider the simple case of spring interaction forces and global communication topology for illustration and ease of analysis; however, these assumptions can be relaxed with predictable effects on the dynamics[35, 47–49].

II. SWARMING PATTERNS AND STABILITY

From generic initial conditions a swarm described by Eq.(1) tends to one of two spatio-temporal patterns: a ring (milling) state, or a rotating state – depending on initial conditions and parameters[46]. The two patterns can be seen in Fig.1(b). Note that the snapshots in time are drawn from simulations of Eq.(1) with Gaussian white-noise, $<\xi_l^{(c)}(t)\,\xi_j^{(c')}(t')>= 0.02\cdot\delta(t-t')\delta_{lj}\delta_{cc'}$, where c and c' denote the Cartesian components, x or y. The emergence and stability of the ring and rotating patterns are often qualitatively described using mean-field approximations, in which the motions of agents relative to the swarm's center-of-mass are neglected[34, 50]. Though useful, such descriptions do not capture bistability and noise-induced switching, let alone the more complex motions observed in experiments[35, 36]. What's more, higher-order approximation techniques predict bistability qualitatively, but suffer from quantitative inaccuracy, and are difficult to analyze[51]. Hence, an analyzable and accurate description of stability is needed, especially for robotics experiments which use Eq.(1) (and its generalizations) as a basic autonomy-controller. In support of such experiments, we analyze the linear stability of the ring and rotating states exactly for large N in the noiseless limit, and compare our predictions to simulations.

A. Ring State

First, since the ring and rotating states are effectively two types of phase-locked solutions with different phase distributions and frequencies, it is useful to transform Eq.(1) into polar coordinates where each can be naturally represented as fixed-point solutions in appropriately chosen rotating reference frames. Introducing the coordinate transformations $\mathbf{r}_l \equiv \langle r_l\cos(\phi_l)\,, r_l\sin(\phi_l)\rangle$, substituting into Eq.(1), and neglecting noise, we obtain:

$$m r_l\ddot{\phi}_l = \left[\alpha - \beta\left(r_l^2\dot{\phi}_l^2 + \dot{r}_l^2\right)\right] r_l\dot{\phi}_l - 2m\dot{r}_l\dot{\phi}_l + \frac{a}{N-1}\sum_{j\neq l} r_j(t-\tau)\sin\left(\phi_j(t-\tau)-\phi_l\right), \tag{2}$$

$$m\ddot{r}_l = \left[\alpha - \beta\left(r_l^2\dot{\phi}_l^2 + \dot{r}_l^2\right)\right]\dot{r}_l + m r_l\dot{\phi}_l^2 + \frac{a}{N-1}\sum_{j\neq l}\left[r_j(t-\tau)\cos\left(\phi_j(t-\tau)-\phi_l\right) - r_l\right]. \tag{3}$$

For large N we can approximate the restricted sums in Eqs.(2-3), over all but one of the agents, with sums over all of the agents. In this case, ring-state formations are solutions of Eqs.(2-3) where radii and frequencies are constant[34], and phases are splayed uniformly,

$$r_j(t) = \sqrt{\frac{m\alpha}{\beta a}}, \qquad \phi_j(t) = \frac{2\pi(j-1)}{N} + \sqrt{\frac{a}{m}}t. \tag{4}$$

This is easy to check by direct substitution. In general, many related ring states also exist, i.e, where some number of agents have the opposite frequency, $-\sqrt{a/m}$, and are distributed uniformly around a concentric ring. In our stability analysis below, we focus on the case where all agents rotate in the same direction for three reasons: this case persists when small repulsive forces are added (as in robotics experiments[35, 36]), the stability of any given ring pattern has only a weak dependence on the number of nodes rotating in each direction (as demonstrated with simulations), and analytical tractability.

To determine the local stability of the ring state we need to understand how small perturbations to Eq.(4)

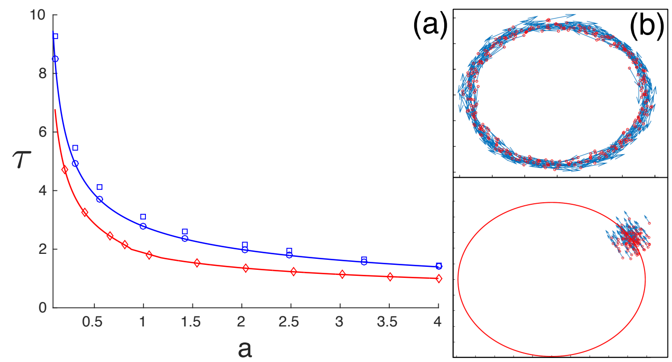

FIG. 1. Stability diagram for delay-coupled swarms. (a) The blue (upper) curve denotes a Hopf bifurcation for the ring state (b, upper). The red (lower) curve denotes a combined line for saddle-node and double-Hopf bifurcations for the rotating state (b, lower). Points denote simulation-determined stability changes for $N = 600$: a ring state with all agents rotating in the same direction (blue circles), a ring state with half the agents rotating in the opposite direction (blue squares), and a rotating state (red diamonds). (b) Snapshots for both states in the x-y plane ($a=1, \tau=2.6$, N=100). Positions are drawn with red circles and velocities with blue arrows. In all panels $m=\alpha=\beta=1$.

grow (or decay) in time. Our first step is to substitute a general perturbation, $r_j(t)=\sqrt{m\alpha/\beta a}+B_j(t)$ and $\phi_j(t) = 2\pi(j-1)/N + \sqrt{a/m}\;t + A_j(t)$, into Eqs.(2-3) and collect terms to first order in $A_j(t)$ and $B_j(t)$ (assuming $|A_j|\,, |B_j| \ll 1\;\forall j$). The result is the following linear system of delay-differential equations for $N \gg 1$ *with constant coefficients* – the latter property is a consequence of our transformation into the proper coordinate system and is what allows for an analytical treatment:

$$\sqrt{\frac{m\alpha}{\beta a}}\left[m\ddot{A}_l + 2\alpha\dot{A}_l\right] + 2\sqrt{\frac{a}{m}}\left[m\dot{B}_l + \alpha B_l\right] = \frac{a}{N}\sum_j\left[B_j^\tau\sin\left(\tfrac{2\pi(j-l)}{N} - \sqrt{\tfrac{a}{m}}\tau\right) + (A_j^\tau - A_l)\sqrt{\frac{m\alpha}{\beta a}}\cos\left(\tfrac{2\pi(j-l)}{N} - \sqrt{\tfrac{a}{m}}\tau\right)\right], \tag{5}$$

$$m\ddot{B}_l - 2m\sqrt{\frac{\alpha}{\beta}}\dot{A}_l = \frac{a}{N}\sum_j\left[B_j^\tau\cos\left(\tfrac{2\pi(j-l)}{N} - \sqrt{\tfrac{a}{m}}\tau\right) - (A_j^\tau - A_l)\sqrt{\frac{m\alpha}{\beta a}}\sin\left(\tfrac{2\pi(j-l)}{N} - \sqrt{\tfrac{a}{m}}\tau\right)\right] \tag{6}$$

where $A_j^\tau \equiv A_j(t-\tau)$ and $B_j^\tau \equiv B_j(t-\tau)$.

Given the periodicity implied by the equally-spaced phase variables in Eq.(4), it is natural to look for eigen-solutions of Eqs.(5-6) in terms of the discrete Fourier transforms of $A_j(t)$ and $B_j(t)$. In fact, by inspection we can see that only the first harmonic survives the summations on the right-hand sides of Eqs.(5-6), because of the sine and cosine terms, and hence we look for particular solutions: $A_j(t) = A\exp\{\lambda t - 2\pi i(j-1)/N\}$ and $B_j(t) = B\exp\{\lambda t - 2\pi i(j-1)/N\}$. Substitution and a fair bit of algebra gives the following transcendental equation for the stability exponent, λ, of the ring state:

$$\frac{m\lambda^2 + 2\alpha\lambda - \frac{a}{2}e^{-\tau\left[\lambda + i\sqrt{\frac{a}{m}}\,\right]}}{2m\sqrt{\frac{a}{m}}\lambda - \frac{a}{2i}e^{-\tau\left[\lambda + i\sqrt{\frac{a}{m}}\,\right]}} + \frac{2\sqrt{\frac{a}{m}}\left[m\lambda + \alpha\right] - \frac{a}{2i}e^{-\tau\left[\lambda + i\sqrt{\frac{a}{m}}\,\right]}}{m\lambda^2 - \frac{a}{2}e^{-\tau\left[\lambda + i\sqrt{\frac{a}{m}}\,\right]}} = 0. \tag{7}$$

In general, the ring state will be linearly stable if there are no solutions to Eq.(7) with $Re[\lambda] > 0$. In fact, varying a and τ while fixing the other parameters, we discover a Hopf bifurcation, generically, at which $\lambda = \pm i\omega_c$ [52]. An example Hopf line is shown in Fig.1(a) in blue for $m = \alpha = \beta = 1$. Based on our analysis, we expect the ring state to be locally stable below the blue line and unstable above it. For comparison, the blue circles in Fig.1(a) denote simulation-determined transition points: the largest $\tau(a)$ for which a swarm of 600 agents, initially prepared in a ring state with a small random perturbation (i.e., independent and uniformly distributed A_j and B_j over $[-10^{-5}, 10^{-5}]$), returns to a ring configuration after an integration time of $t = 20000$. Numerical predictions from Eq.(7) show excellent agreement with these simulation results. Similarly determined transition points for a ring formation in which half the agents rotate in one direction, and half rotate in the opposite direction, are shown with blue squares. We can see that the ring's Hopf-transition line still gives a good approximation for this more general case, especially for larger values of a.

In addition to the transition points, we can check the frequency of oscillations around the ring state, implied by the existence of an unstable mode for $\tau(a)$ slightly above the Hopf bifurcation. First we perform a simulation initially prepared in the ring state with a small perturbation (as described in the preceding paragraph), and compute the peak frequency, ω^*, in the Fourier spectrum of the swarm's center-of-mass, $\mathbf{R}(t) \equiv \sum_j \mathbf{r}_j/N$. An example is shown in the inlet panel of Fig.2(a) for $(a = 3.243, \tau = 1.565)$; the symbol P denotes the absolute value of the Fourier transform. Second, we plot $\omega_c = \omega^* - \sqrt{a/m}$ and compare to predictions from solutions of Eq.(7) with $\lambda = \pm i\omega_c \neq 0$ for a range of time delays. The comparison is shown in Fig.2(a) with excellent agreement.

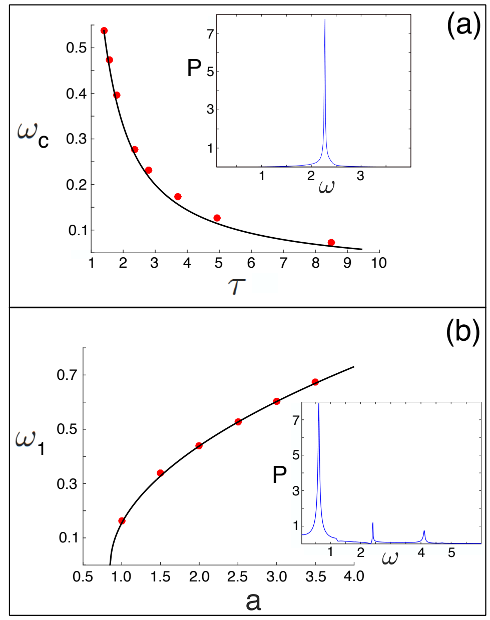

FIG. 2. Frequency of unstable modes near bifurcation. (a) unstable frequency for the ring state at the Hopf bifurcation (black line) determined from the power spectrum of the swarm's center-of-mass (red circles). (b) unstable frequency for the rotating state at the double-Hopf bifurcation (black line) determined from the power spectrum for a single agent. Inlet panels show example spectra for both states: (a) when $(a = 3.243, \tau = 1.565)$, (b) when $(a = 3.5, \tau = 1.059)$. In all panels $m = \alpha = \beta = 1$.

B. Rotating State

Next, we perform a similar stability analysis for the rotating state, which has a different bifurcation structure and unstable modes. Unlike the ring state, the rotating state entails a collapse of the swarm on to the center of mass with complete phase and amplitude synchronization (in the noiseless limit). In polar coordinates, the agents satisfy $r_j(t) = R$ and $\phi_j(t) = \Omega t$ [34], where

$$0 = m\Omega^2 - a\left[1 - \cos\Omega\tau\right], \tag{8}$$

$$R = \frac{1}{|\Omega|}\sqrt{\frac{\alpha - a\sin(\Omega\tau)/\Omega}{\beta}}. \tag{9}$$

In order to determine the local stability of the rotating state we substitute $r_j(t) = R + B_j\exp\{\lambda t\}$ and $\phi_j(t) = \Omega\, t + A_j\exp\{\lambda t\}$, into Eqs.(2-3) and, again, collect terms to first order in A_j and B_j (assuming $|A_j|, |B_j| \ll 1\ \forall j$). The result is another linear system of equations with constant coefficients. After some algebra, and replacing the restricted sums in Eqs.(2-3) by sums over all particles, we obtain:

$$R\big[m\lambda^2 - \lambda(\alpha - 3\beta R^2\Omega^2) + a\cos(\Omega\tau)\big]A_l + \Omega\big[2m\lambda - \alpha + 3\beta R^2\Omega^2\big]B_l = \frac{ae^{-\lambda\tau}}{N}\sum_j \Big[R\cos(\Omega\tau)A_j - \sin(\Omega\tau)B_j\Big], \quad (10)$$

$$\big[aR\sin(\Omega\tau) - 2mR\Omega\lambda\big]A_l + \big[m\lambda^2 - m\Omega^2 - \lambda(\alpha - \beta R^2\Omega^2) + a\big]B_l = \frac{ae^{-\lambda\tau}}{N}\sum_j \Big[R\sin(\Omega\tau)A_j + \cos(\Omega\tau)B_j\Big]. \quad (11)$$

There are two primary categories of solutions to Eqs.(10-11). The first is $A_l = A$ and $B_l = B$, which we call the homogeneous modes. Because all agents move together (equal to the the center-of-mass motion) the stability entailed by the homogeneous modes should match the mean-field approximation mentioned above and analyzed in[34]. Because the mean-field is known to be quantitatively inaccurate for capturing stability[36, 51], we focus on the second set of solutions: $\sum_j A_j/N = 0$ and $\sum_j B_j/N = 0$. The stability-exponents, λ, for these modes satisfy

$$\frac{2m\Omega\lambda - a\sin(\Omega\tau)}{m\lambda^2 - \lambda(\alpha - 3\beta R^2\Omega^2) + a\cos(\Omega\tau)} - \frac{m\lambda^2 - m\Omega^2 - \lambda(\alpha - \beta R^2\Omega^2) + a}{\Omega\big[\alpha - 3\beta R^2\Omega^2 - 2m\lambda\big]} = 0. \quad (12)$$

Equation (12) has four complex solutions.

In general, the rotating state will be linearly stable if there are no solutions to Eq.(12) with $Re[\lambda] > 0$. In practice, we find that changing a and τ while keeping all other parameters fixed, produces saddle-node, Hopf and double-Hopf bifurcations[52–54]. In the former case, a single real eigenvalue approaches zero, when

$$\tan(\Omega\tau) = \frac{m\Omega^2 - a}{\Omega(\alpha - 3\beta R^2\Omega^2)} \;. \quad (13)$$

Equation (13) gives the stability-line for the rotating state with small a and large τ. For large a and small τ, the stability changes through a double-Hopf bifurcation where two frequencies become unstable simultaneously, $\lambda = \pm i\omega_1,\ \pm i\omega_2 \neq 0$. Fig.1(a) shows the predicted composite stability-curve for the rotating state, combining both bifurcations. Plotted is the maximum τ, for fixed a, where $Re[\lambda] > 0$. Above the red line the rotating state is expected to be locally stable, and below it, unstable (see Sec.IV for an enlarged view of the bifurcation curves for the rotating state).

As with the ring state, we compare our stability predictions to simulations, and determine the smallest value of $\tau(a)$ for which a swarm of $N = 600$ agents, initially prepared in the rotating state with a small, random perturbation, returns to a rotating state after a time of $t = 20000$. These points are shown with red diamonds in Fig.1(a) for several values of coupling. Again, we find excellent agreement with predictions. Another consequence of our analysis is the clear quantitative prediction of swarm bistability (between the red and blue curves in Fig.1) and noise-induced switching between ring and rotating patterns, which can now be precisely tested in experiments[35, 36, 40].

Lastly, just as with the ring state, we can compare the frequency of oscillations around the rotating state for $\tau(a)$ slightly below the double-Hopf bifurcation values, where we expect weak instability of modes orthogonal to the center-of-mass-motion. First we perform a simulation initially prepared in the rotating state with a small perturbation, and compute the peak frequency, ω^*, in the Fourier spectrum of $r_j - R$, where j is a randomly selected agent. An example is shown in the inlet panel of Fig.2(b) for ($a = 3.5$, $\tau = 1.059$). This peak frequency is compared to predictions from numerical solutions of Eq.(12) with $\lambda = \pm i\omega_1,\ \pm i\omega_2 \neq 0$ for a range of coupling strengths. In Fig.2(b) the smaller of the two frequencies, ω_1 is plotted along with ω^* – showing excellent agreement. Note that in this comparison, we do not subtract off the rotating state's frequency, Ω, since r_j does not oscillate in the rotating state but is equal to R.

III. CONCLUSION

In this work we studied the stability of ring and rotational patterns in a general swarming model with time-delayed interactions. We found that ring states change stability through Hopf bifurcations, where spatially periodic modes sustain oscillations in time. On the other hand, rotating states undergo saddle-node, Hopf, and double-Hopf bifurcations, where modes with orthogonal dynamics to the center-of-mass-motion change stability. For both states, the unstable oscillations correspond to dynamics not captured by standard mean-field approximations. Our results were verified in detail with large-agent simulations. Future work will extend our analysis to include the effects of repulsive forces, noise, and incomplete (and dynamic) communication topology – all of which are necessary for parametrically controlling real swarms of mobile robots.

JH, IT, and IBS were supported by the U.S. Naval Research Laboratory funding (N0001419WX00055) and the Office of Naval Research (N0001419WX01166) and (N0001419WX01322). TE was supported through the U.S Naval Research Laboratory Karles Fellowship. SK

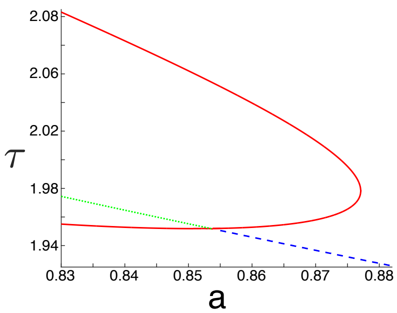

FIG. 3. Bifurcation curves for the rotating state near the intersection of saddle-node (red line), Hopf (green dotted line), and double-Hopf (blue dashed line) bifurcations. Other parameters are $m = \alpha = \beta = 1$.

was supported through the GMU Provost PhD award as part of the Industrial Immersion Program

IV. APPENDIX

Close inspection of Fig.1(a), shows that there is a small, apparent discontinuity in the stability line for the rotating state. This apparent discontinuity is a consequence of several bifurcation curves intersecting in a small region in the (a, τ) plane for $m = \alpha = \beta = 1$. For completeness, we show an enlarged version of the bifurcation curves for the rotating state in Fig.3. The rotating state is linearly stable in the region to the right of the red line (saddle-node) and blue dashed line (double-Hopf) bifurcations. The combined stability line drawn in Fig.1 for the rotating state, plots whichever value of τ is larger between the red and blue-dashed curves in Fig.3, *for each value of a*. Note that the blue dashed curve in Fig.3 is a bifurcation of the rotating state and is different from the blue curve in Fig.1(a).

[1] K. Tunstrm, Y. Katz, C. C. Ioannou, C. Huepe, M. J. Lutz, and I. D. Couzin, PLoS. Comput. Biol. **9**, 1 (2013).

[2] D. S. Calovi, U. Lopez, S. Ngo, C. Sire, H. Chaté, and G. Theraulaz, New Journal of Physics **16**, 015026 (2014).

[3] A. Cavagna, L. Del Castello, I. Giardina, T. Grigera, A. Jelic, S. Melillo, T. Mora, L. Parisi, E. Silvestri, M. Viale, and A. M. Walczak, Journal of Statistical Physics **158**, 601 (2015).

[4] G. F. Young, L. Scardovi, A. Cavagna, I. Giardina, and N. E. Leonard, PLoS Comput. Biol. **9**, 1 (2013).

[5] M. Ballerini, N. Cabibbo, R. Candelier, A. Cavagna, E. Cisbani, I. Giardina, V. Lecomte, A. Orlandi, G. Parisi, A. Procaccini, M. Viale, and V. Zdravkovic, Proc. Natl. Acad. Sci. U.S.A **105**, 1232 (2008).

[6] H. Ling, M. G. E., van der Vaart K., V. R. T., T. A., and N. T. Ouellette, R. Soc. B. **286** (2019), 10.1098/rspb.2019.0865.

[7] J. Li and A. H. Sayed, EURASIP Journal on Advances in Signal Processing **2012**, 18 (2012).

[8] G. Theraulaz, E. Bonabeau, S. C. Nicolis, R. V. Solé, V. Fourcassié, S. Blanco, R. Fournier, J.-L. Joly, P. Fernández, A. Grimal, P. Dalle, and J.-L. Deneubourg, Proc. Natl. Acad. Sci. U.S.A **99**, 9645 (2002).

[9] C. M. Topaz, M. R. D'Orsogna, L. Edelstein-Keshet, and A. J. Bernoff, PLoS Comput. Biol. **8**, 1 (2012).

[10] A. Polezhaev, R. Pashkov, A. I. Lobanov, and I. B. Petrov, Int. J. Dev. Bio. **50**, 309 (2006).

[11] K. Rio and W. H. Warren, Transportation Research Procedia **2**, 132 (2014), the Conference on Pedestrian and Evacuation Dynamics 2014 (PED 2014), 22-24 October 2014, Delft, The Netherlands.

[12] T. Vicsek and A. Zafeiris, Phys. Rep. **517**, 71 (2012).

[13] M. C. Marchetti, J. F. Joanny, S. Ramaswamy, T. B. Liverpool, J. Prost, M. Rao, and R. A. Simha, Rev. Mod. Phys. **85**, 1143 (2013).

[14] M. Aldana, V. Dossetti, C. Huepe, V. M. Kenkre, and H. Larralde, Phys. Rev. Letts. **98**, 095702 (2007).

[15] M. Brambilla, E. Ferrante, M. Birattari, and M. Dorigo, Swarm Intelligence **7**, 1 (2013).

[16] L. Bayndr, Neurocomputing **172**, 292 (2016).

[17] P. Bandyopadhyay, IEEE Trans. Ocean. Engr. **30**, 109 (2005).

[18] W. Wu, Automatica **47**, 2044 (2011).

[19] R. K. Ramachandran, K. Elamvazhuthi, and S. Berman, "An optimal control approach to mapping gps-denied environments using a stochastic robotic swarm," in *Robotics Research: Volume 1*, edited by A. Bicchi and W. Burgard (Springer International Publishing, Cham, 2018) pp. 477–493.

[20] D. S. Morgan and I. B. Schwartz, Physics Letters A **340**, 121 (2005).

[21] J. Wiech, V. A. Eremeyev, and I. Giorgio, Continuum Mechanics and Thermodynamics **30**, 1091 (2018).

[22] H. Li, C. Feng, H. Ehrhard, Y. Shen, B. Cobos, F. Zhang, K. Elamvazhuthi, S. Berman, M. Haberland, and A. L. Bertozzi, in *2017 IEEE/RSJ International Conference on Intelligent Robots and Systems (IROS)* (2017) pp. 4341–4347.

[23] H. G. Tanner, A. Jadbabaie, and G. J. Pappas, IEEE Transactions on Automatic Control **52**, 863 (2007).

[24] V. Gazi, IEEE Transactions on Robotics **21**, 1208 (2005).

[25] A. Jadbabaie, Jie Lin, and A. S. Morse, IEEE Transactions on Automatic Control **48**, 988 (2003).

[26] C. Virágh, G. Vásárhelyi, N. Tarcai, T. Szrényi, G. Somorjai, T. Nepusz, and T. Vicsek, Bioinspiration & Biomimetics **9**, 025012 (2014).

[27] J. P. Desai, J. P. Ostrowski, and V. Kumar, in *IEEE Transactions on Robotics and Automation*, Vol. 17(6) (2001) pp. 905–908.

[28] L. Giuggioli, T. McKetterick, and M. Holderied, PLoS Comput. Biol. **11** (2015).

[29] N. Nagy, Z. Akos, D. Biro, and T. Vicsek, Nature **464**, 890 (2010).

[30] L. Jiang, L. Giuggioli, A. Perna, and et. al., PLoS Comput. Biol. **13**, e1005822 (2017).

[31] J. Fehrenbach, J. Narski, J. Hua, S. Lemercier, A. Jelic, C. Appert-Rolland, S. Donikian, J. Pettr, and P. Degond, (2014), 10.3934/nhm.2015.10.579, arXiv:1412.7537.

[32] M. Komareji, Y. Shang, and R. Bouffanais, Nonlinear Dynamics **93**, 1287 (2018).

[33] L. Oliveira, L. Almeida, and P. Lima, in *2015 IEEE World Conference on Factory Communication Systems (WFCS)* (2015) pp. 1–8.

[34] L. M. y Teran-Romero, E. Forgoston, and I. B. Schwartz, IEEE Transactions on Robotics **28**, 1034 (2012).

[35] K. Szwaykowska, I. B. Schwartz, L. Mier-y Teran Romero, C. R. Heckman, D. Mox, and M. A. Hsieh, Phys. Rev. E **93**, 032307 (2016).

[36] V. Edwards, P. deZonia, M. A. Hsieh, J. Hindes, I. Triandof, and I. B. Schwartz, *Delay-Induced Swarm Pattern Bifurcations in Mixed-Reality Experiments*, Chaos [under review].

[37] H. Hartle and R. Wackerbauer, Phys. Rev. E **96**, 032223 (2017).

[38] G. Ansmann, K. Lehnertz, and U. Feudel, Phys. Rev. X **6**, 011030 (2016).

[39] J. Hindes and M. Assaf, Phys. Rev. Lett. **123**, 068301 (2019).

[40] K. Szwaykowska, I. B. Schwartz, and T. W. Carr, in *11th International Symposium on Mechatronics and its Applications (ISMA)* (2018) pp. 1–6.

[41] D. Kularatne, E. Forgoston, and M. A. Hsieh, Chaos **29**, 053128 (2019).

[42] J. Hindes and I. B. Schwartz, Chaos **28**, 071106 (2018).

[43] H. Levine, W. J. Rappel, and I. Cohen, Phys. Rev. E **63**, 017101 (2000).

[44] U. Erdmann, W. Ebeling, and A. S. Mikhailov, Phys. Rev. E **71**, 051904 (2005).

[45] M. R. D'Orsogna, Y. L. Chuang, A. L. Bertozzi, and L. S. Chayes, Phys. Rev. Lett. **96**, 104302 (2006).

[46] E. Forgoston and I. B. Schwartz, Phys. Rev. E **77**, 035203(R) (2008).

[47] Y. Chuang, M. D'Orsogna, D. Marthaler, A. Bertozzi, and L. Chayes, Physica D **232**, 33 (2007).

[48] A. Bernoff and C. Topaz, SIAM Journal of Applied Dynamical Systems **10**, 212 (2011).

[49] J. Hindes, K. Szwaykowska, and I. B. Schwartz, Phys. Rev. E **94**, 032306 (2016).

[50] B. Lindley, L. Mier-y-Teran-Romero, and I. B. Schwartz, in *2013 American Control Conference* (2013) pp. 4587–4591.

[51] L. M. y Teran-Romero and I. B. Schwartz, EPL **105**, 20002 (2014).

[52] Y. A. Kuznetsov, *Elements of Applied Bifurcation Theory* (Springer, Berlin, 2004).

[53] Because the stability analysis is performed in rotating frames of reference, technically the Hopf bifurcations are torus bifurcations, and the saddle-node bifurcations are saddle-nodes-of-periodic-orbits.

[54] J. Hindes and C. R. Myers, Chaos **25**, 073119 (2015).